water

MDPI

Article

Particle Dynamics in Ushuaia Bay (Tierra del Fuego)-Potential Effect on Dissolved Oxygen Depletion

Ximena Flores Melo [1,*], Jacobo Martín [1], Lounes Kerdel [2], François Bourrin [2], Cristina Beatriz Colloca [3], Christophe Menniti [2] and Xavier Durrieu de Madron [2,*]

[1] Laboratorio de Oceanografía, Centro Austral de Investigaciones Científicas (CADIC-CONICET), Bernardo Houssay 200, V9410CAB Ushuaia, Argentina; jmartincadic@gmail.com

[2] CEFREM, CNRS, Université de Perpignan Via Domitia, 52 avenue Paul Alduy, 66860 Perpignan, France; kerdellounis@gmail.com (L.K.); fbourrin@univ-perp.fr (F.B.); menniti@univ-perp.fr (C.M.)

[3] Institute of Polar Sciences, Natural Resources and Environment, Universidad Nacional de Tierra del Fuego, Fuegia Basket 251, V9410BXE Ushuaia, Argentina; ccolloca@untdf.edu.ar

* Correspondence: ximenaflores@cadic-conicet.gob.ar (X.F.M.); demadron@univ-perp.fr (X.D.d.M.)

Received: 21 December 2019; Accepted: 19 January 2020; Published: 22 January 2020

Abstract: This study examines the distribution and seasonal evolution of hydrographic, hydrodynamic, and nepheloid layers in Ushuaia Bay and the submerged glacial valley that connects it to the Beagle Channel. The hydrographic structure is highly seasonal, with a total mixing of the water column in winter and the appearance of a pycnocline between 50 and 70 m deep from spring to late autumn, mainly due to desalination. A counter-clockwise current sweeps the entire bay regardless of the season or phase of the tide. This current is at its maximum in the surface layer, allowing the rapid renewal of the bay's waters, while deep currents are weak and imply a slow renewal of the valley's waters. Turbid and oxygen-depleted structures are observed in summer in the valley. The combination of seasonal stratification, high organic matter inputs from planktonic production, oxygen consumption for remineralization, and sluggish circulation results in a decrease in near-bottom oxygen concentration in the glacial valley at the end of the stratified season, before mixing and re-oxygenation of the water column during the southern winter. The possible impact of dissolved oxygen depletion in the bottom waters of the valley on benthic organisms, like crustaceans, is discussed.

Keywords: Beagle Channel; Ushuaia Bay; hydrology; suspended particulate matter; hypoxia

1. Introduction

1.1. Hypoxia in the Coastal Zone

Continental margins play a crucial role in global ocean carbon cycling through the in situ production, resuspension, transport by lateral advection, and transformation during their path to the seafloor [1]. About 10 percent of the world's population lives in coastal areas (www.un.org) and they are related to many human activities that make this area complicated and vulnerable.

In semi-closed basins, estuaries, and fjords, the oxygen regime is regulated by the supply of organic matter (OM), its rate of consumption, the periodicity of water exchange, bathymetric features, and seasonal stratification. In some cases, they may present a substantial depletion of dissolved oxygen (DO) in their deepest zones [2,3]. Dissolved oxygen concentrations below thresholds that compromise the health of marine ecosystems, a condition known as hypoxia, have been studied thoroughly around the world because of its environmental and economic consequences [4]. While a hypoxia threshold of 2 mg/L is commonly adopted, [5] determine hypoxia as a crucial oxygen concentration below ~4.7 mg/L for some benthic species, such as crustaceans. Such oxygen-depleted conditions imply a loss in biodiversity and an impact on the surviving organisms, a reduction of their growth and reproduction, a generation of physiologic stress, forced migrations, a reduction of suitable habitat, increased vulnerability to predation, and a disruption of life cycles [3,6].

High-latitude fjords and channels are known as areas prone to hypoxic conditions due to the synergy between vertical stratification (brought about by active freshwater contribution), and sharp bathymetric discontinuities that may promote a sluggish water renewal [2,7].

1.2. Study Area

The Beagle Channel (Figure 1) is located in the southern extreme of America. Linking the Austral Pacific and Atlantic Oceans as a continuous conduit between them and being 180 km west-east long, it is characterized by a glacially carved channel, which was utterly ice-covered during the last glaciation and flooded by the sea circa 8000 years BP [8,9].

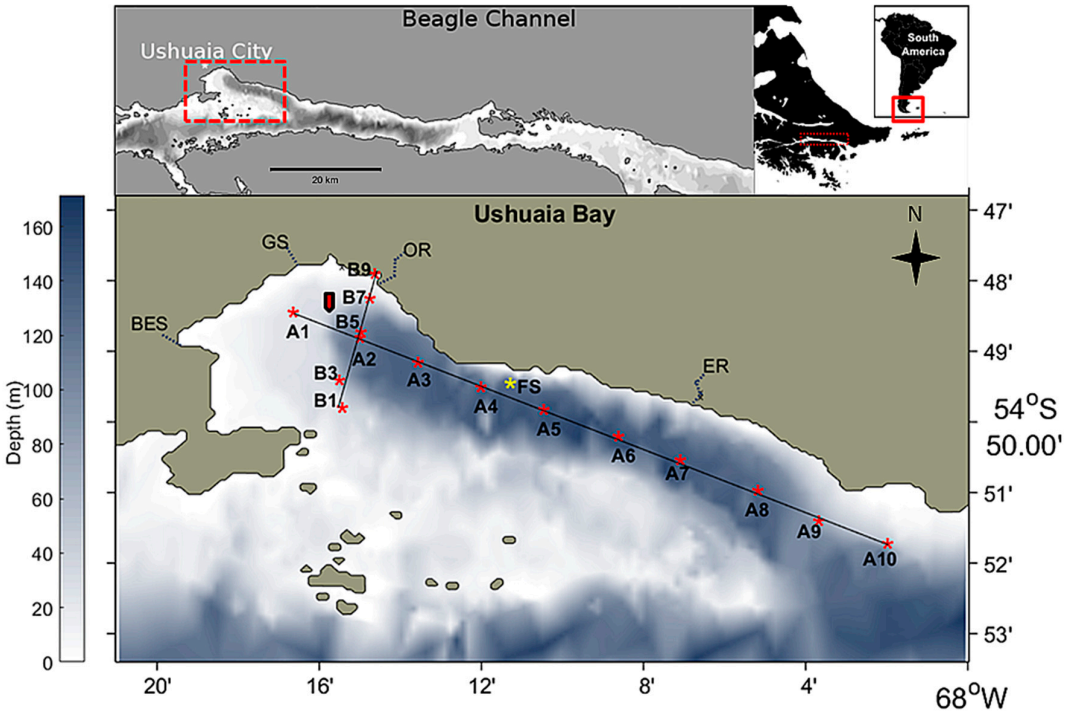

Figure 1. Map of the study area located in Tierra del Fuego, South America (upper right panel), as a branching of the Beagle Channel (upper left panel). Bathymetry in the Ushuaia Bay and its valley (lower panel) is in a grey-white color gradient. Cross-Bay section (B1–B9 stations) from 54°50.088′ S–68°15.710′ W to the 54°47.992′ S–68°14.781′ W, linking the western peninsula with the river mouth of the Rio Olivia, Along Bay section (A1–A10 stations) from 54°48.500′ S–68°16.800′ W to 54°49.595′ S–68°12.183′ W and Fixed Station (FS in yellow) are represented. The freshwater inputs are indicated: BES (Buena Esperanza stream), GS (Grande Stream), OR (Olivia River) and ER (Escondido River).

This high latitude system (~55° S) has a marked seasonal cycle, with maximal air temperatures (5–14 °C) and runoff during austral summer, and minimal temperature (−1 °C–5 °C) during winter [10]. The tidal regime corresponds with a mixed semidiurnal, with tidal amplitudes in the range 0.67–2.18 m, and 1.2 m in average [11]. The prevailing SW winds reach 31 km/h on average [10].

The bathymetry of the Beagle Channel is complex and irregular, consisting of a series of shallow sills and deeper basins. This condition, together with large freshwater inputs, has led previous authors (e.g., [8,12]) to view the entire Beagle Channel as a semi-estuarine marine environment that displays a fjord-like circulation.

The Ushuaia Bay (Figure 1) is located on the north coast of the Beagle Channel. The bay displays a northwest-southeast orientation and can be roughly divided into a western sector with a smooth bathymetry, reaching 10–30 m depth and an eastern area where depth increases sharply, continuing with a U-shaped, drowned glacial valley with an average depth of 150 m along its axis. Based on modeling, the residual water circulation has been described as an anti-clockwise gyre [11].

The bay receives freshwater discharges from the Olivia, Arroyo Grande, Encajonado and Buena Esperanza rivers, having annual average discharges of 5, 35, 1.3 (only winter data), and 0.9 m^3/s respectively [10,13]. The city of Ushuaia

(54°48′ S, 68°19′ W) is located along the northern part of the Bay. This city and its port have undergone substantial growth in recent decades, resulting in a significant anthropogenic pressure from discharges of urban and industrial effluents [14]. A sewage diffuser is situated on the eastern coast with the wastewater from the city [13].

Previous studies in this area [15] showed minimum values of oxygen in the deepest zone of Ushuaia Bay during the austral autumn and early winter of 2015, reaching DO concentrations around 3 mg/L in June at the head of the glacial valley. This near-bottom oxygen depletion was associated to seasonal vertical stratification that isolates the deeper water masses from contact with the atmosphere, thus preventing its ventilation [15].

This works aim at characterizing the interplay of hydrographic features, water circulation, and particle matter distribution and composition in Ushuaia Bay and adjacent valley and assess their potential role in regulating DO concentrations. The study embraces three contrasting periods of the year: austral winter (August), summer (January) and autumn (April), along which residual currents, suspended particle concentration and size distribution, particulate organic carbon (POC) content and fluorescence of chlorophyll-a (Chl-a fluorescence; as a proxy for phytoplankton biomass) were measured to constrain the forcings that may drive oxygen depletion in the study area.

2. Materials and Methods

2.1. Sampling Strategy

The measurement strategy had two components (Table 1). Firstly, a 1.5-year-long (August 2017 to December 2018) quasi-monthly monitoring of the hydrology at a fixed station, 150 m deep, located in the valley (FS in Figure 1). This point was chosen considering that it represents a transitional place between the Beagle Channel and Ushuaia Bay, being part of the deep glacial valley. The variables measured included physical (temperature, salinity, density) and bio-optical (DO, Chl-a fluorescence, turbidity) parameters. Secondly, spatial monitoring of hydrological and hydrodynamic structures across and along the axis of the bay and valley (Figure 1) was carried out in winter (August 2017), summer (January 2018) and autumn (April 2018). Additional data on the concentration and size of suspended particles and POC concentration were also acquired during that period.

Table 1. List of parameters collected at the fixed station and along the sections. (*) monthly sampling limited to December 2017–December 2018 period.

Parameter	Instrument	Period			
		August 2017 December 2018	August 2017	January 2018	April 2018
Temperature, Salinity, Density, Oxygen, Turbidity, Fluorescence	CTD	Fixed station	Cross Bay (B1–B8)	Cross Bay (B1–B8)	Cross Bay (B1–B9) Along Bay (A1–A10)
Particle size spectra	LISST-100X	-	Cross Bay (B1–B8)	Cross Bay (B1–B8)	Cross Bay (B1–B9)

Particle images	LISST-Holo	-	Cross Bay (B1–B8)	-	-
Currents	ADCP	-	Cross Bay (B1–B8)	-	Cross Bay (B1–B9)
POC	Niskin bottle	Fixed station (*)	-	-	-

2.2. Hydrological Data

A multiparameter JFE ASTD 102 RINKO profiler was used to collect surface to bottom profiles at 10 Hz of pressure, temperature, conductivity, DO, Chl-a fluorescence, and turbidity data. DO was measured with a fast-responding fluorescence sensor. The oxygen sensor was adjusted routinely following a two-point calibration (0% in Na_2SO_3 solution; 100% bubbled water for 30 min) as recommended by the manufacturer. Additionally, water samples were collected at selected depths during surveys using a Niskin bottle, to conduct oxygen analysis by Winkler titration

$$\text{Winkler DO (mg/L)} = 0.81 \times \text{DO sensor } (R^2 = 0.96, N = 27).$$

Chl-a fluorescence concentration and turbidity were measured with a fluorometer and a backscattering sensor, respectively. Raw data were transformed into engineering units using the software and calibration sheets provided by the manufacturer and later processed using the Sea-Bird Data Processing Software to obtain 1-dbar binned data. Derived parameters (potential temperature, salinity, potential density anomaly, density ratio) were derived according to the TEOS-10 equations. Hydrographic data were processed according to routine procedures and displayed using the Ocean Data View software [16].

On several occasions, near-bottom water samples were collected together with CTD profiles and filtered on 0.4 μm Whatman Nuclepore Polycarbonate filters. In situ volumetric concentrations of suspended particulate material (SPM) were estimated from dry weights of particulate matter. A simple regression equation was derived between SPM concentration and turbidity measurements for the optical backscatter sensor:

$$\text{SPM(mg/L)} = 1.17 \times \text{Turbidity(FTU)} + 0.25 \ (R^2 = 0.88, N = 17),$$

which can be used to approximate the observed concentrations.

2.3. In Situ Particle Size and Shape

A Sequoia LISST-100X (Type C, 2.5–500 μm range, 1 Hz sampling rate) was used together with the CTD (Conductivity, Temperature and Depth) probe to estimate the in situ particle size distribution (PSD) in the water column.

PSD was derived from the laser diffraction spectrum using the "randomly shaped" Mie's theory [17–19]. The raw spectrum was converted into volume concentration (expressed in μL/L) using the volume conversion constant. Extreme size classes (1.90–2.25 and 322–381 μm) showed typical "rising tails" explained by the presence of smaller particles (for the first class) and bigger particles (for the last class) outside the measurement range [20]. Except for the LISST-100X primary

particle characterization in the laboratory, we excluded the extreme size classes of the PSD measured in situ before calculating the derived parameters (total volume concentration, Vctot). PSDs were then normalized with Vctot and expressed in %.

During the August 2017 survey, a digital holographic camera (Sequoia LISST-HOLO, 0.2 Hz sampling rate) was used in parallel to the LISST-100X to study the volume and number concentrations, and the shape of large particles, within the range 20–2000 μm [21]. Two steps of 5 min, 2 m below the surface and 2 m above the bottom were carried out for each profile to collect enough images (>150), which were combined to obtain a representative estimation of particle composition in the surface bottom layers. PSD was estimated using a Matlab based image analysis processing (based on the estimate of the spherical equivalent diameter), and the size spectrum was expressed in μL/L for each of the 50 size classes logarithmically spaced from 20 to 2000 μm. The LISST-HOLO also measured several particle shape parameters. The aspect ratio (AR = length of minor axis/length of major axis), and the equivalent circular diameter (ECD) were used to classify the particles.

2.4. Particulate Organic Carbon Concentrations

Monthly water samples were taken with Niskin bottles at three levels between December 2017 and December 2018 (except June and August 2018) at the fixed station (FS in Figure 1), water samples were collected close to the surface, around the deep Chl-a fluorescence maximum (at about 20 m) and close to the seafloor. Suspended particle matter (SPM) concentrations were determined by filtering seawater on GF/F filters (0.7 μm nominal pore size) following the method described in [22]. Filters were then used to determine particulate organic carbon (POC) content. Firstly, dry samples were decarbonated with repeated additions of H_3PO_4 (1M) and HCl (2M) until the end of effervescence. POC contents were then measured using a VarioMAX CN, Elementar (Langenselbold, Germany) Instrument.

2.5. Hydrodynamical Data

A Teledyne RDI workhorse 300 KHz ADCP was used to measure currents along the cross-bay section (B1–B9 in Figure 1). The ADCP was mounted on an aluminum structure attached to a dinghy, which moved at a speed between 1 and 2 m/s along the section. The boat's trajectory was tracked by GPS. The ADCP was programmed to sample at 1 Hz with a vertical resolution of 4 m, and took measurements of current speed and direction from 7 m depth to 4–8 m above the bottom (signals from the 4 ADCP beams, each with an orthogonal angle of 20°, are typically affected by side-lobe interference in the lowest 6% of the depth). The section was repeated 4 to 5 times resulting in cross-profiles 3950–4250 m and 36–63 min long. For operational reasons, each survey could not extend beyond 5 h and cover a complete tidal cycle. It used the bottom tracking to derive absolute speed and direction, and bottom depth. Velocity data were linearly extrapolated in the unmeasured zones to the bed and the surface.

Data from the different transects were projected on the average cross-section plane using an orthogonal translation and interpolated on a regular grid. The arithmetic average of the velocity components of all transects was computed at each node of the grid. Water discharge was calculated as the flow perpendicular to the mean cross-section.

The renewal time in the northern part of Ushuaia Bay delimited by the section was estimated as the ratio of the volume of the domain (evaluated at 3.4×10^8 m^3 by integrating bathymetric data interpolated on a regular grid) and the water flow entering the bay and perpendicular to the section.

A short-term mooring line was deployed between 2 December and 11 December 2019 on a 60 m bottom in the valley axis (54°48.316 S–68°14.972 W, Figure 1) to describe the variability of tidal currents and determine the residual current at the water vein entering the shallow bay. The currents were measured with a Nortek Aquadopp acoustic current meter, positioned at a depth of 4 m, with 2 min burst sampling at 1 Hz every 10 min.

The tidal data (sea-level anomaly) are from the Ushuaia gauging station maintained by the Argentinian Naval Hydrographic Service and have been retrieved from the IOC sea-level station monitoring facility (http://www.ioc-sealevelmonitoring.org/).

3. Results

3.1. Temporal Variability of Hydrology: 2014–2018 Time Series at the Fixed Station

As other high latitudes systems, the hydrographical structure of the Ushuaia Bay shows the seasonal stratification over the year (Figure 2). During austral summer, approximately from December to March, stratification results from the presence of warmer (T > 8 °C) and fresher (S < 30) surface layer, with respect to the deep layer (T = 5–7° C, S = 31–32). The pycnocline is around 40–70 m depth, with a density anomaly about 22 kg/m^3 at the surface and 25 kg/m^3 close to the bottom. During winter, from April to November, the water column becomes homogeneous with temperatures around 5–7 °C, salinity around 31–32, and density anomalies around 24.8–25 kg/m^3. As a general rule, DO depletion (<6 mg/L) occurs after the seasonal stratification. The oxygen decline is seen during autumn, starting in April and reaching minimal values in June. During August, the vertical mixing allows the oxygen to increase along the water column reaching values between 9 and 11 mg/L. The largest oxygen depletion is found after the summer of 2015, reaching concentration around 3.7 mg/L during June, in water deeper than 136 m.

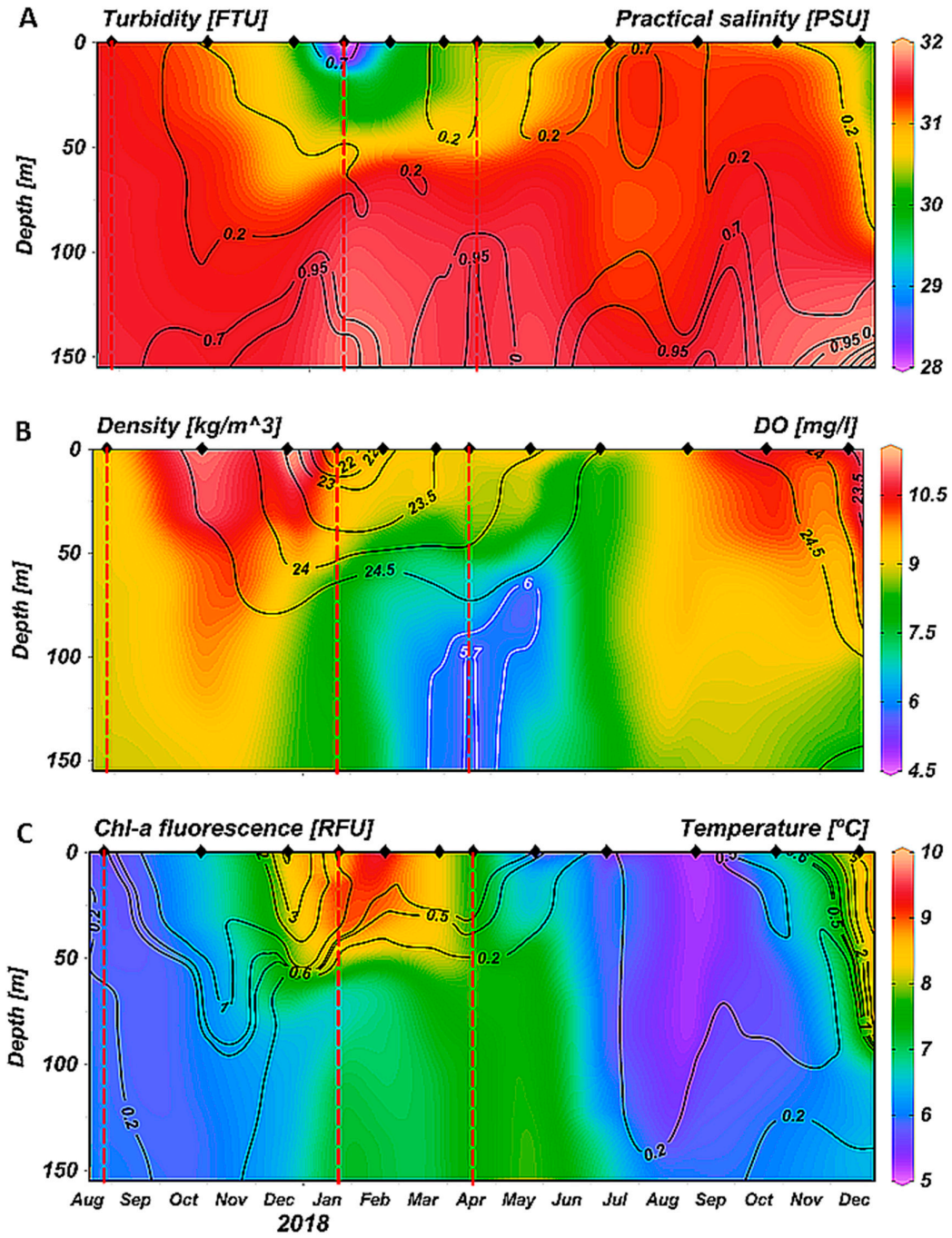

Figure 2. Time series at the fixed station over the entire water column measured between August 2017 and December 2018 of (**A**) salinity (in gradient color) and turbidity (black isolines); (**B**) dissolved oxygen (in gradient color and white isolines) and density anomaly (black isolines); and (**C**) temperature (in gradient color) and Chl-a fluorescence (black isolines). The enhanced observation period: red dotted lines are the field trips of August 2017, January 2018, and April 2018.

Monitoring was carried out at the fixed station in December 2017 and December 2018, the concentrations of POC on the surface and subsurface covary with the

fluorescence of Chl-a 5 (Figure 3A). These two variables have an unambiguous seasonal signal with maximum values of POC (21–22 µM C) and Chl-a fluorescence (4 RFU, Relative Fluorescence Unit) in December and minimum values of POC (4 µM C) and Chl-a fluorescence (0.2 RFU) in May–June.

During the same period, POC concentrations at the bottom of the valley (Figure 3B) show distinct variability with the first maximum in December (17 µM C), associated with high DO concentration (9 mg/L), and a second relative maximum of POC in March (12 µM C) preceding the annual DO minimum (5.5 mg/L).

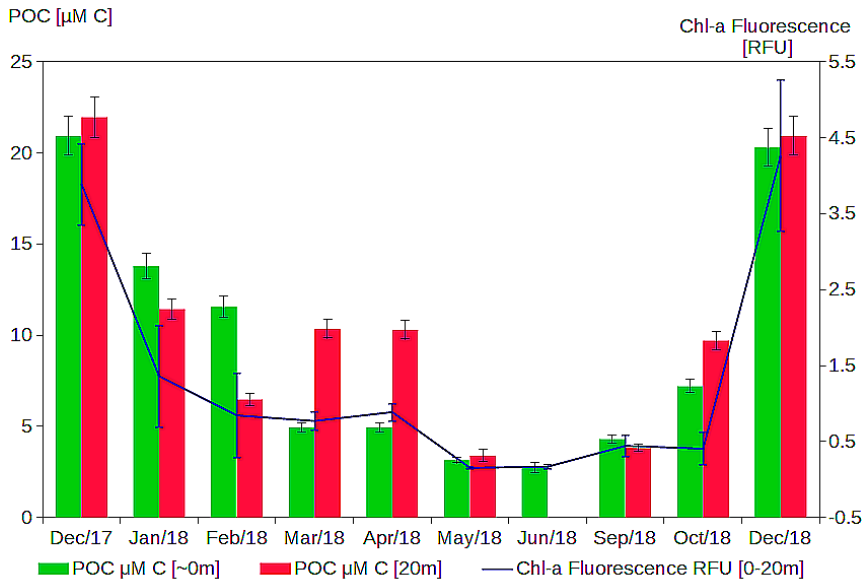

(**A**)

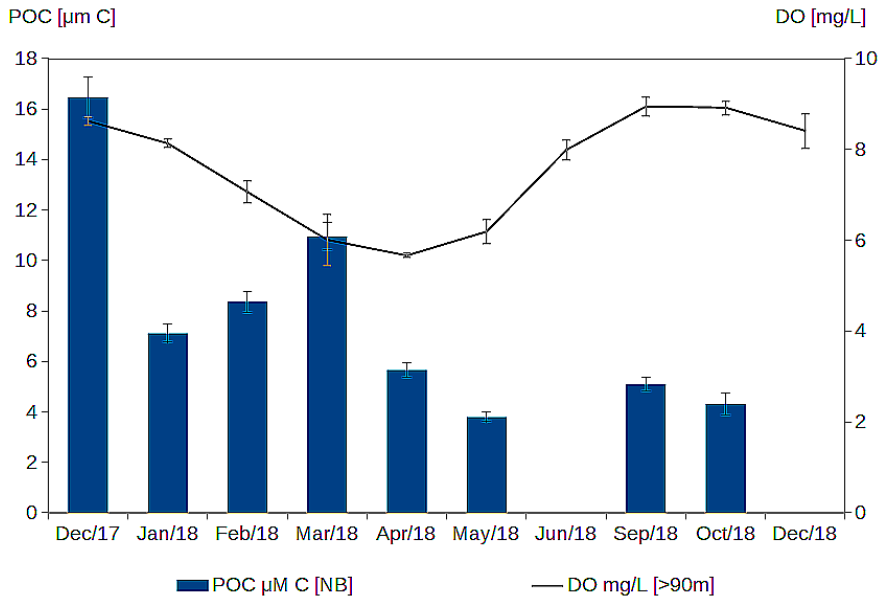

(**B**)

Figure 3. Time series between December 2017 and December 2018 at the fixed station (FS in Figure 1) of (**A**) POC concentrations at the surface (S) and subsurface (SS, 20 m depth) together with the averaged Chl-a fluorescence concentrations between 0 and 20 m deep; (**B**) POC concentrations near the bottom (NB) and averaged DO concentrations for depths over 90 m.

3.2. Spatial Variability of Hydrology: Seasonal Sections Across and Along the Ushuaia Bay and Valley

Observations along the sections (Figures 4–7) characterize the spatial extent of hydrological structures across the bay and valley at critical times of the year (winter, summer, autumn).

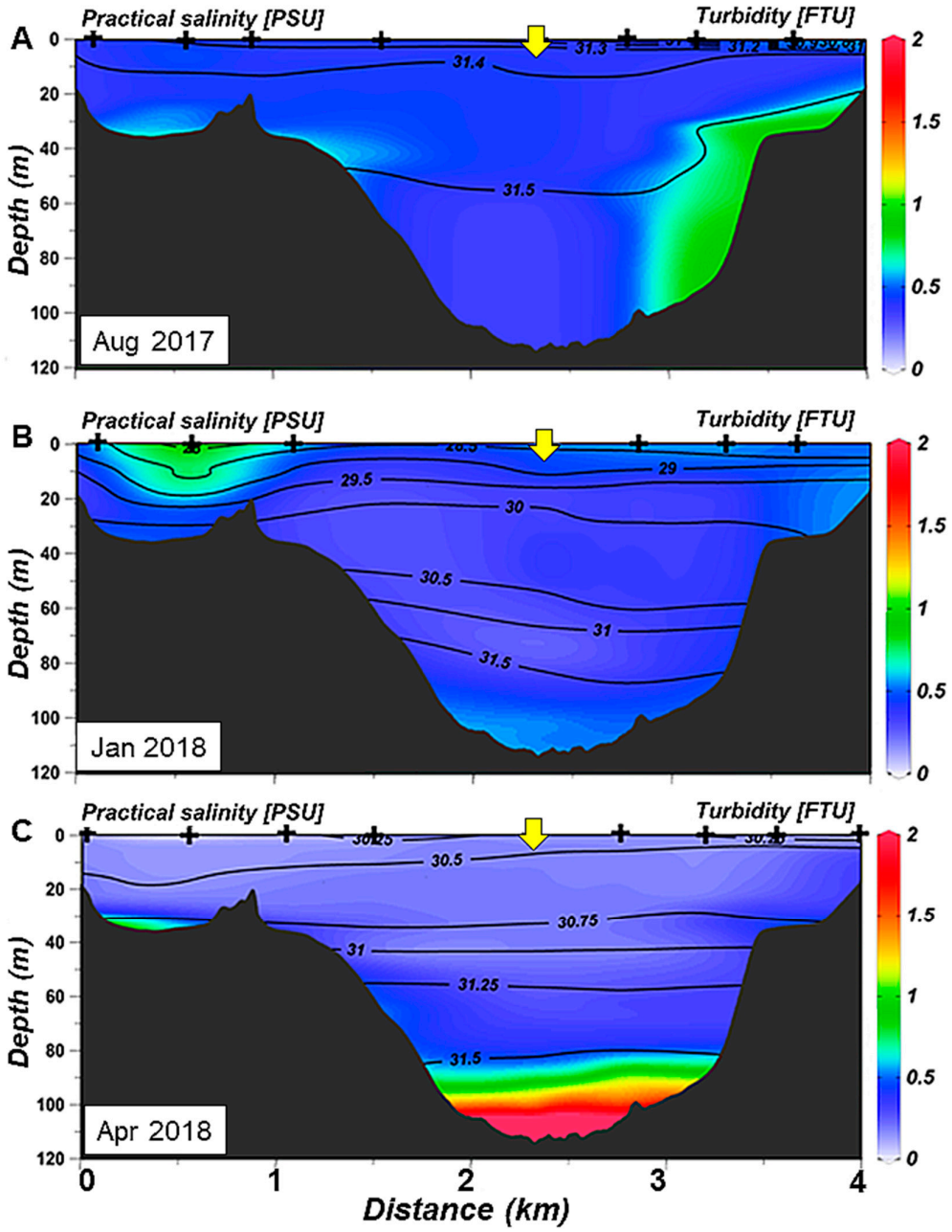

Figure 4. Cross-bay section of turbidity (color gradient) and salinity (isolines) for (**A**) August 2017; (**B**) January 2018; and (**C**) April 2018. The intersection between cross-bay and along-bay sections is marked with a yellow arrow.

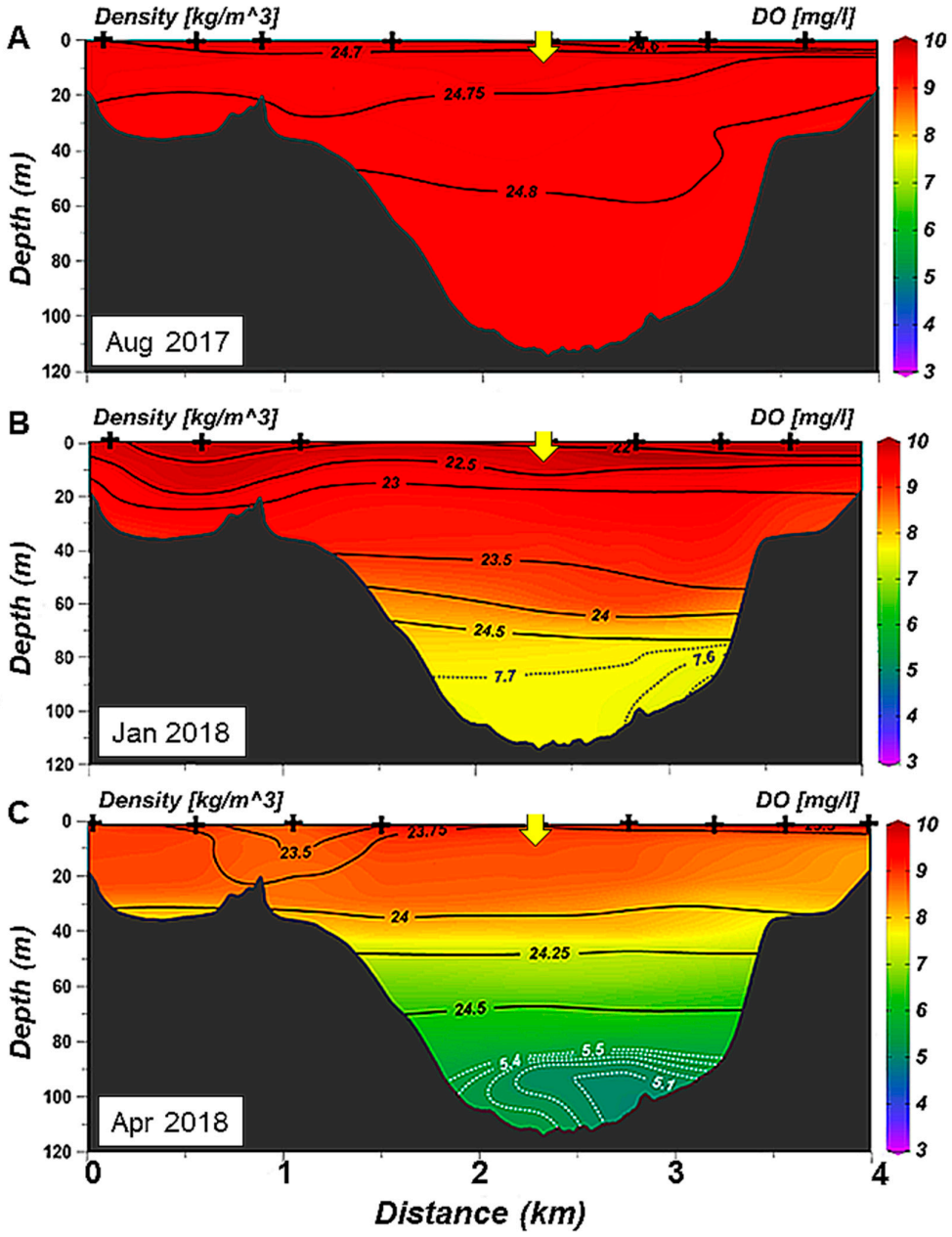

Figure 5. Cross-bay section of DO (color gradient and white isolines at the bottom) and density anomaly (isolines) for (**A**) August 2017; (**B**) January 2018; and (**C**) April 2018. The intersection between cross-bay and along-bay sections is marked with a yellow arrow.

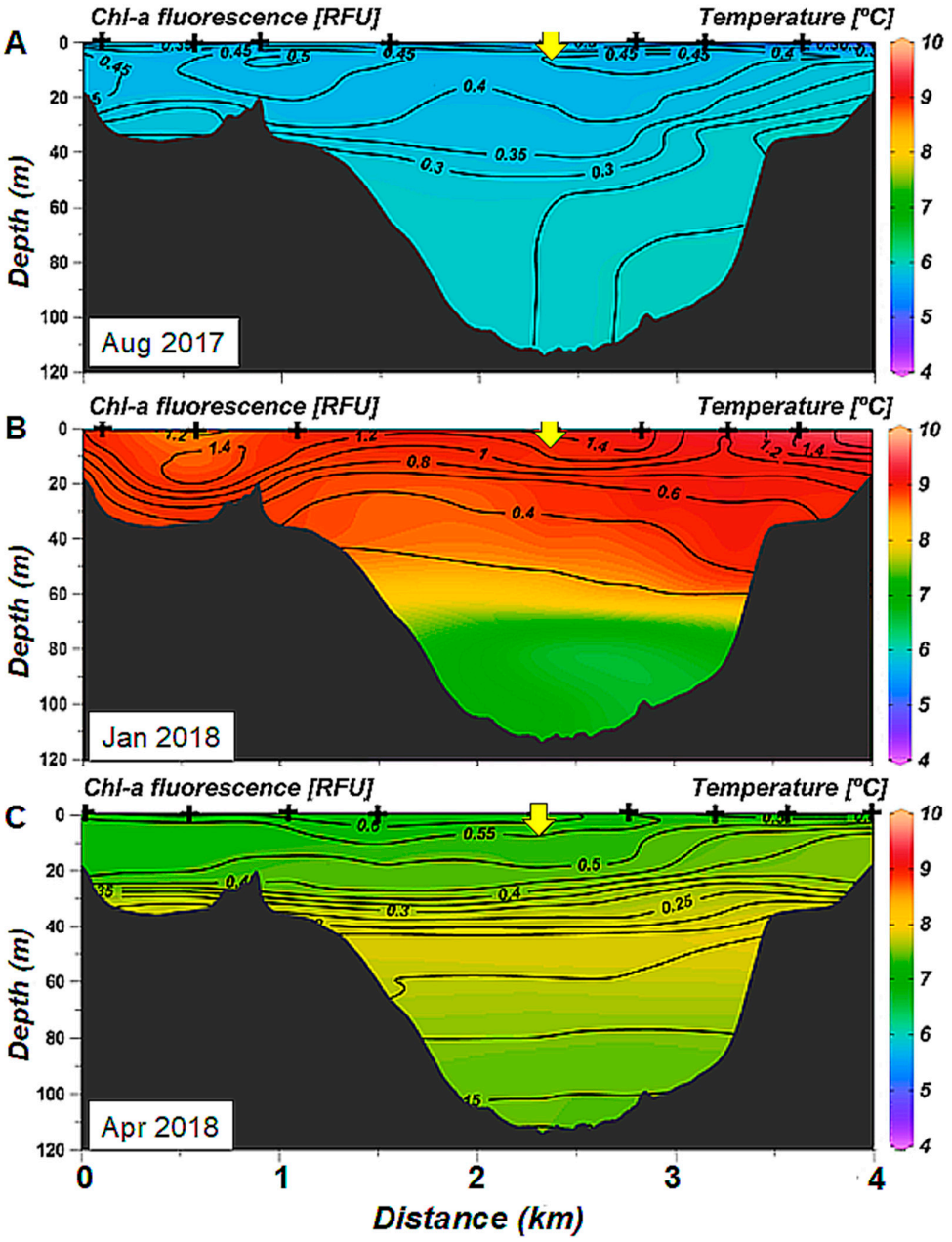

Figure 6. Cross-bay section of temperature (color gradient) and Chl-a fluorescence (isolines) for (**A**) August 2017; (**B**) January 2018; and (**C**) April 2018. The intersection between cross-bay and along-bay sections is marked with a yellow arrow.

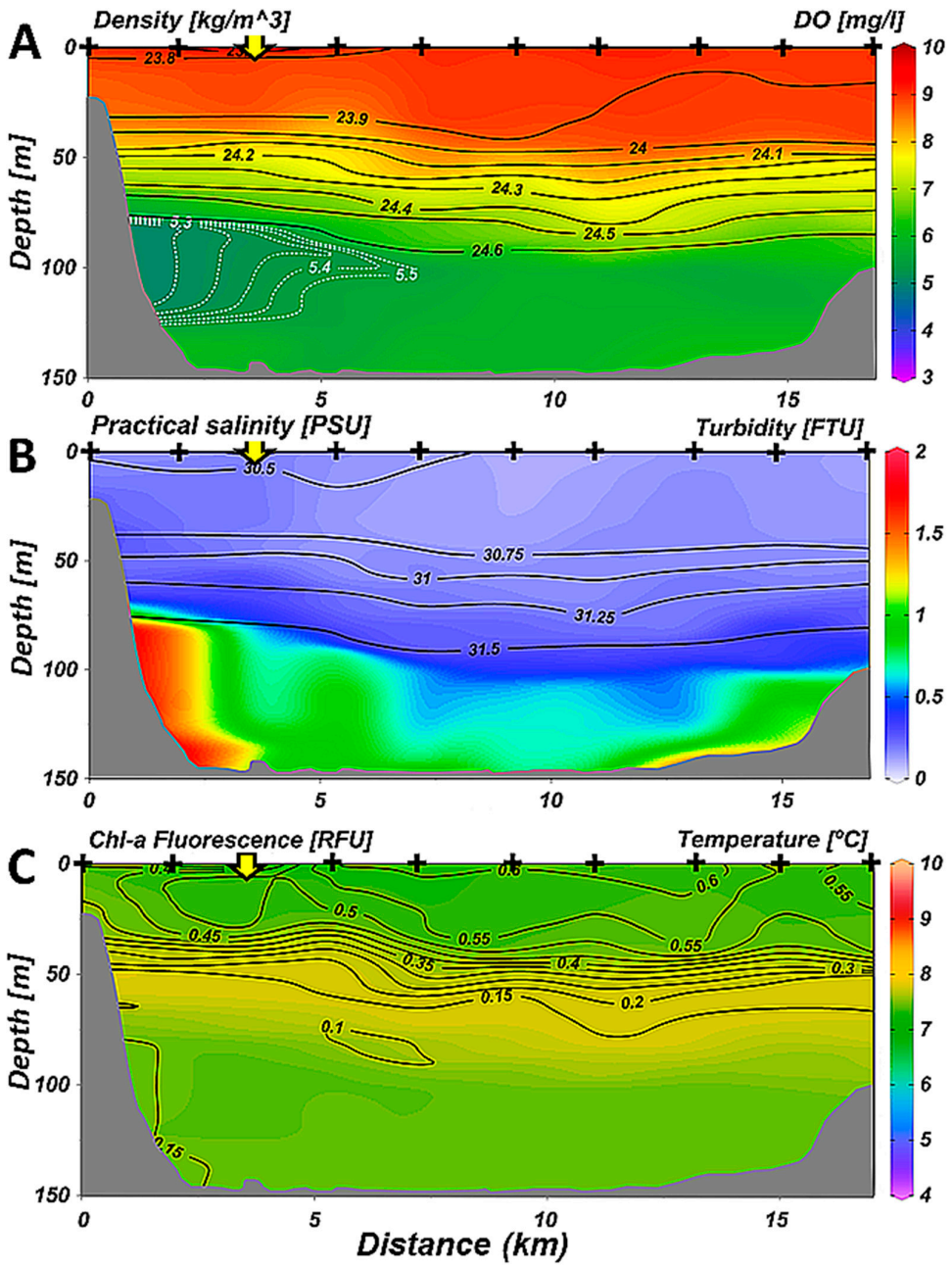

Figure 7. Along-bay section of (**A**) DO (in gradient color and white dotted isolines) and density anomaly (black isolines); (**B**) turbidity (in gradient color) and salinity (black isolines); and (**C**) temperature (in gradient color) and Chl-a fluorescence (black isolines) for April 2018. The intersection between cross-bay and along-bay sections is marked with a yellow arrow.

As previously described in Figure 2, observations made in August 2017 (Figures 4A, 5A and 6A) clearly illustrate the effect of winter mixing, which results in near-homogenization of the entire water column for all parameters, except for turbidity, which shows an increase near the bottom of the bay and on the eastern side of the valley.

In January (Figures 4B, 5B and 6B), the thermohaline stratification is maximum with minimal salinity and maximum temperature in the surface layer that is delimited by a pycnocline at a depth of 60 m.

In April, structures both across the bay (Figures 4C, 5C and 6C) and along the valley (Figure 7) show that stratification remains important despite the cooling and desalination of the surface layer. The decrease in DO in the deep layer intensifies during the stratified period and the minimum oxygen, located at the bottom of the valley and near the bay in April, corresponds to the maximum turbidity. Chl-a fluorescence values indicate that phytoplankton production is reduced but still active and located above the pycnocline level.

The low values of Chl-a fluorescence in the turbid bottom layers, in both stratified and non-stratified periods, indicate that the SPM is probably composed of senescent planktonic particles.

3.3. Particulate Matter Characteristics

Three distinct layers are considered to estimate and illustrate the evolution of the in situ size spectrum of suspended particles in the water column and for the different seasons (Figure 8). Since the horizontal variations in size spectra do not vary significantly, and to obtain an integrated view, data from all stations in the section across the bay were combined for each layer. The layers retained are the surface layer (0–20 m), the layer around the seasonal pycnocline (40–70 m) and the bottom layer in the valley (90 m–bottom).

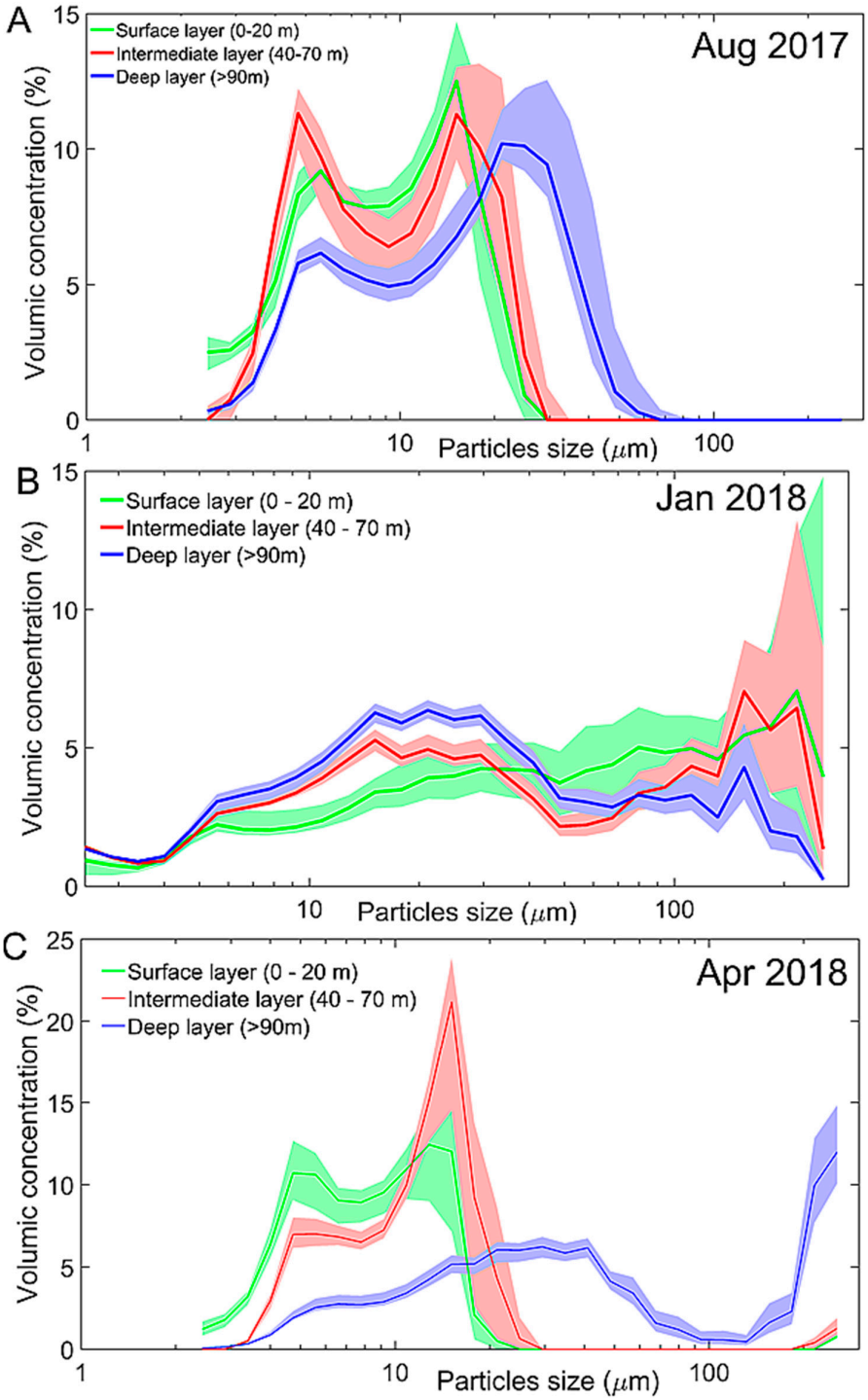

Figure 8. PSD in the surface (green, 0–20 m), intermediate (red, 40–70 m) and deep (blue, 90 m–bottom) layers for all stations of the section across the bay for (**A**) August 2017; (**B**) January 2018; and (**C**) April 2018. The thick lines represent the median values, and the light-colored envelopes represent the 25% and 75% percentiles.

The size spectra in winter (August 2017; Figure 8A) shows strong similarities. The first mode around 5 μm appears on the entire water column. The second mode is around 15 μm in the surface and intermediate layers and increased slightly, about 20 μm, at depth. In summer (January 2018, Figure 8B), during the planktonic

bloom period, the size spectra change significantly, although they still have two main modes. The first mode between 10 and 40 µm appears in the intermediate and deep layers, while the second mode between 150 and 250 µm appears at all levels. In the fall (April 2018, Figure 8C), the size spectra differ depending on the depth. While the surface and intermediate layers show a bi-modal size spectrum, close to that of the previous winter, with a mode around 5 µm and another around 15 µm, the size spectrum in the deep layer presents characteristics close to summer, with a secondary mode between 10 and 40 m and a main mode composed of particles larger than 150 µm.

The particle assemblage image (Figure 9A) corresponding to the surface layer in August 2017 shows that the in situ particle population is dominated by small aggregates with sizes ranging between 0 and 120 µm with a large variability of shapes (AR between 0.1 and 1). In the bottom layer (Figure 9C), the in situ particle population is also dominated by a large proportion of fine particles but the imaging system shows large aggregates ranging from 120 to 300 µm.

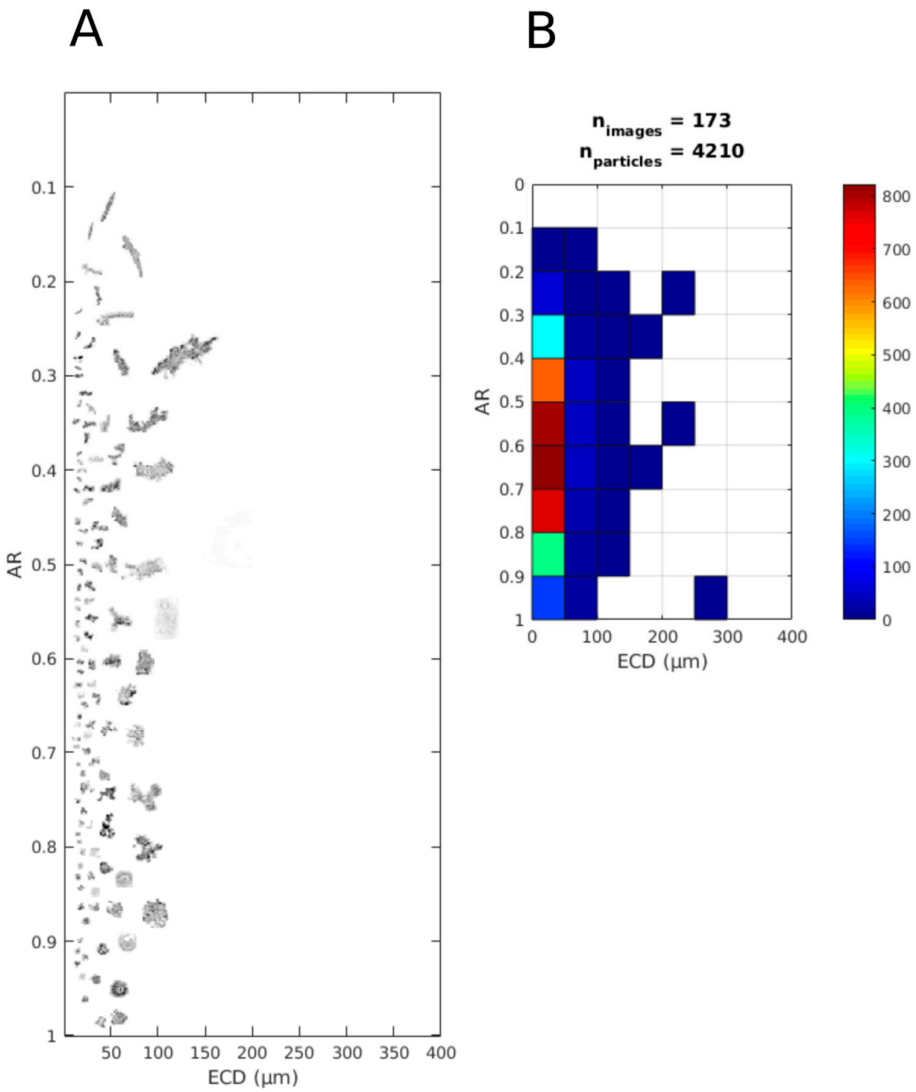

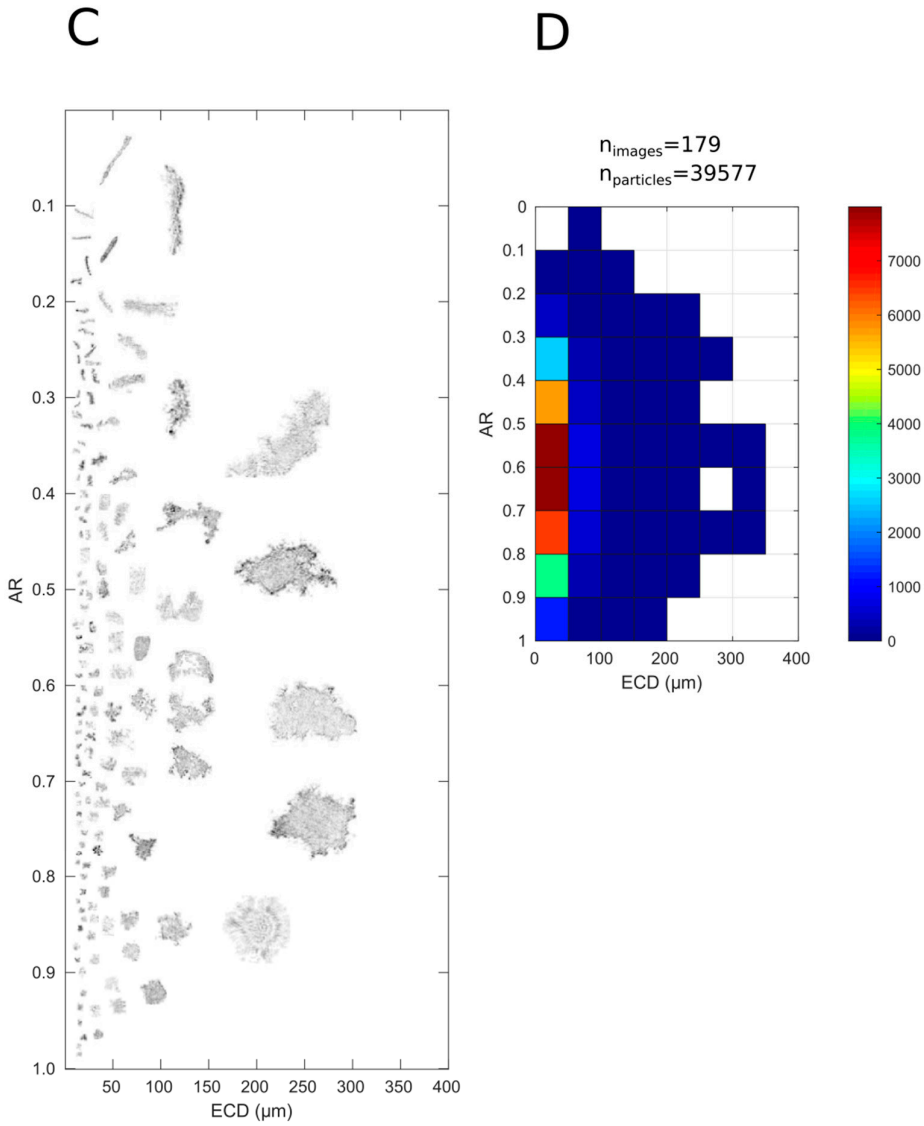

Figure 9. Examples of particle assemblages from the LISST-HOLO images (**A**) at the surface and (**C**) near the bottom for all stations of the across-bay section in August 2017. Variation of SPM aspect ratio (AR, dimensionless) as a function of the SPM equivalent circular diameter (ECD, µm) at the surface (**B**) and the bottom layer (**D**). The corresponding particle number distribution per size class is shown on the right panels.

The maximum density of particles in both surface and bottom layers is found in the 0–50 µm size classes with AR (aspect ratio) ranging from 0.5 to 0.7 (Figure 9B,D). The number of measured particles from approximately the same number of analyzed images in both layers (173–179 images) shows that the particle number concentration is one order of magnitude larger in the bottom layer than in the surface layer.

3.4. Currents Intensity and Variability

Currents were measured across the bay in two seasons (August 2017 and April 2018) around the high tide period associated with the predominant semidiurnal tidal cycle (Figure 10A,B) to take into account its effect on the circulation and renewal of the bay and valley waters. In addition, and in order to have information on the complete tidal cycle, single-point current meter measurements were obtained for eight days (between 2 December and 11 December 2019) in the shallow part of the valley (see mooring position in Figure 1).

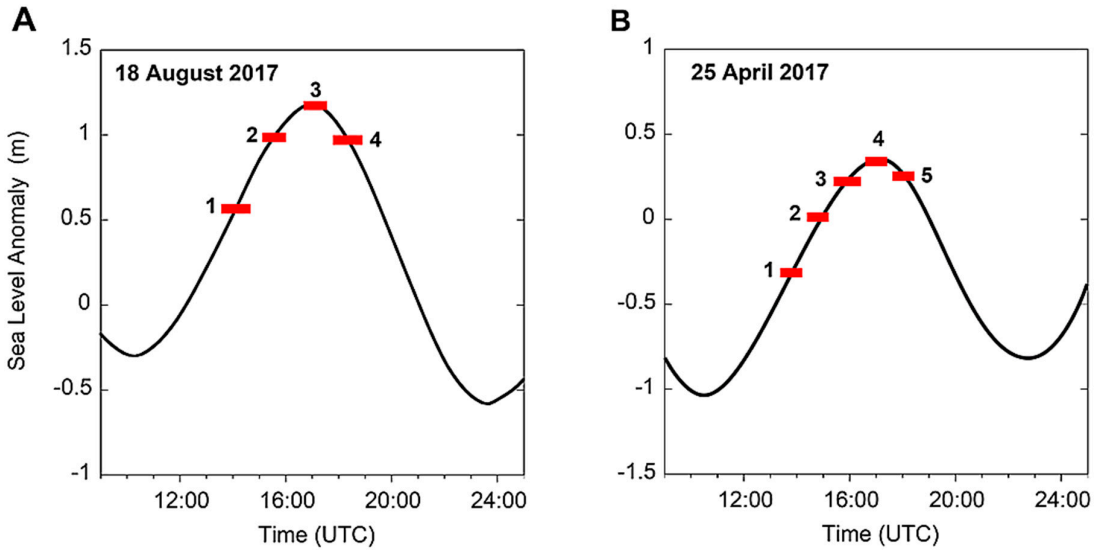

Figure 10. Time of the ADCP cross-bay sections performed in winter (**A**, August 2017), and autumn (**B**, April 2018). Numbers are the successive sampled sections in the different tidal moments. Tidal parameters were obtained from http://www.hidro.gov.ar/oceanografia/Tmareas/RE_Mareas.asp.

The average currents for the high sea period during the stratified and non-stratified seasons are similar and are mainly perpendicular to the section (Figure 11). They clearly show that the circulation in the bay during the flood and high tide periods is counter-clockwise at the surface over a thickness of 50 m. The intensity of the average currents is 6–7 cm/s at the surface and decreases with depth. The mean speed is about 3 cm/s. Minimal current speed is found in the deep layer of the valley (1–3 cm/s).

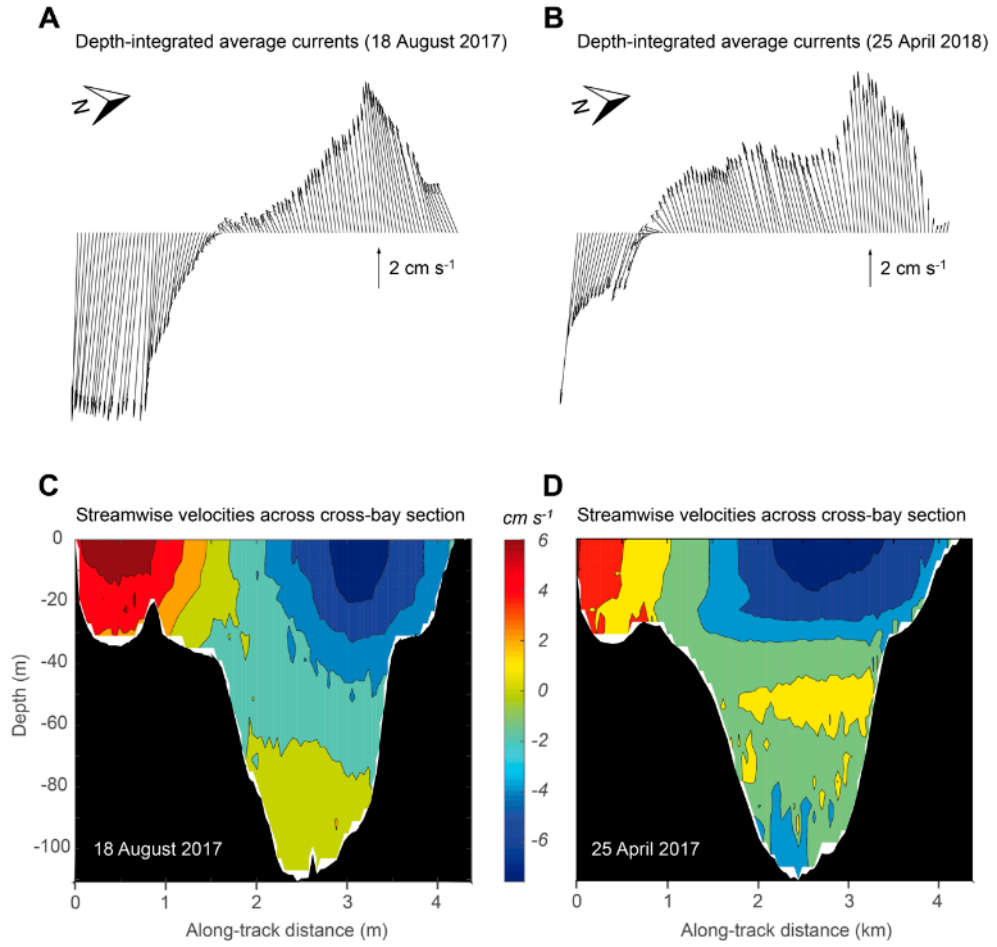

Figure 11. Current intensity and direction along the section across the bay for (**A**) August 2017 and (**B**) April 2018. The sections were repeated over part of the tidal cycle and covered periods of flow and ebb. The side views of the sections for (**C**) August 2017 and (**D**) April 2018 show the magnitude of the currents normal to the section, entering and leaving the bay, averaged over the different crossings. The top views show the depth-integrated currents along the section averaged over the various passages in both seasons.

Short term mooring results (Figure 12A,B) clearly shows that the current is aligned mainly along the axis of the valley, with maximum velocities of 20 cm/s, and that the residual current, which is about 7 cm/s, is oriented towards the W-NW (286° N) and corresponds to the main vein entering the bay. The semidiurnal tidal currents are low (<2 cm/s). This result complements the one of [23], which showed that the tidal currents and residual current at the southwestern end of the transect were oriented towards the east-southeast.

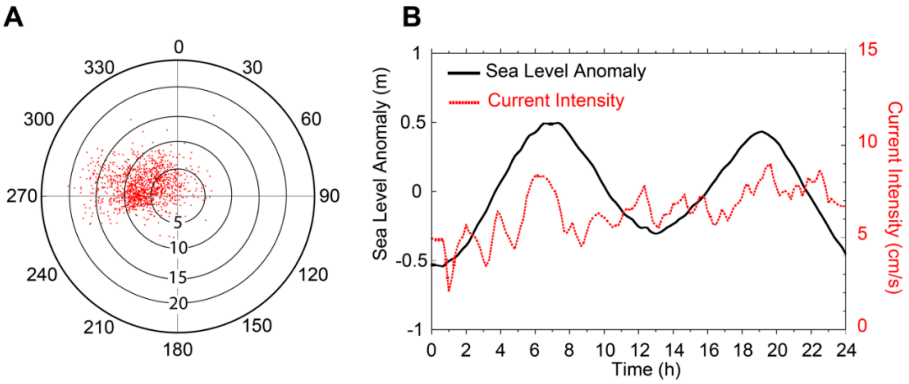

Figure 12. (**A**) Scatter plot of the short term current meter data from December 2 to December 10, 2019; and (**B**) average daily sea-level anomaly and current intensity along the mean current direction.

Hence, the results from the different transects and the short-term mooring show that the predominant semidiurnal tides only slightly modulate the currents and that the residual current clearly indicates that the average circulation in the bay is counter-clockwise. The average water flow entering the bay in the first 50 m of the water column and contributing to the renewal of its waters is estimated at ~3 × 10^3 m^3/s in August 2017 and ~6 × 10^3 m^3/s in April 2018 (Table 2). Considering a volume of the Ushuaia bay of 2.05 × 10^8 m^3, the residence time of the waters in the bay varies between 9 h (August 2017) and 19 h (April 2018). The sluggish currents in the valley likely imply a slower renewal and ventilation of the deep waters.

Table 2. Date, time, and inflow in the first 50 m of the water column for the ADCP cross-bay sections performed in winter (August 2017), and Autumn (April 2018).

18 August 2017	25 April 2018
	13:19–14:10 UTC
	Flood: High Tide − 3 h 00
	Inflow: 4.5 × 10^3 m^3/s
14:10–14:40 UTC	14:33–15:13 UTC
Flood: High Tide − 2 h 00	Flood: High Tide − 2 h 00
Inflow: 3.3 × 10^3 m^3/s	Inflow: 4.7 × 10^3 m^3/s
15:11–15:59 UTC	15:33–16:18 UTC
Flood: High Tide − 1 h 00	Flood: High Tide − 1 h 00
Inflow: 4.1 × 10^3 m^3/s	Inflow: 5.2 × 10^3 m^3/s
16:44–17:30 UTC	16:43–17:19 UTC
Slack water: High Tide	Slack water: High Tide
Inflow: 3.2 × 10^3 m^3/s	Inflow: 3.50 × 10^3 m^3/s
17:58–18:46 UTC	17:41–18:21 UTC
Ebb: High Tide + 1 h 00	Ebb: High Tide + 1 h 00
Inflow: 3.1 × 10^3 m^3/s	Inflow: 2.6 × 10^3 m^3/s

4. Discussion

Our monitoring in the Ushuaia Bay shows a clear seasonal stratification, with the presence of a thermocline, halocline, and pycnocline at a depth of 50 and 70 m from December to March. The stratification observed in the Ushuaia Bay and its

valley during the warm season is primarily attributed to the freshwater inputs coming from the surrounding mountains, which remain covered by ice and snow during winter [13]. Even if during summer, the enhanced solar radiation [10] could play a primary role on the surface layer warming, desalination is the predominant factor in the establishment of seasonal stratification, as in other similar environments such as the nearby fjords and channels of the Magellan region of Chile [24].

At the same time that summer stratification is established due to freshwater runoff, a phytoplankton biomass maximum appears in the surface layer as indicated by the highest concentrations of Chl-a fluorescence and POC between December and February. The particulate material present in the surface layer up to the pycnocline level is then mainly formed by coarse particles that are composed of either planktonic organisms or aggregates. The major tributaries rivers of the Ushuaia Bay are the Olivia and Grande rivers. These rivers drain soils rich in organic matter, such as peat bogs and forests, and one of them (GS) also transports untreated industrial and urban effluents. They induce an enrichment in nutrients and OM of the bay [13]. However, this impact appears to be limited to the shallow environments of the bay [25], suggesting that the particulate organic matter reaching the deep layer in the valley is mainly the result of settling of the OM produced in the surface layer rather than the transport of particulate organic matter from the rivers.

While the entire water column is well ventilated and almost saturated in DO (95%) in winter (May-September), there is a significant decrease in DO in the bottom layer, to an average of 70% saturation, during the summer (November–February) and fall (March–April) periods associated to the largest POC concentrations (Figure 3B). The DO in the deep layer decreases notably in the head of the valley (Figures 5C and 7A), where bottom water renewal is probably the longest. During summer and fall, the pycnocline inhibits vertical mixing and reoxygenation of the deep layer, while settling of the aggregated OM produced in the surface layer is maximum (Figure 3). The DO in the deep layer reaches minimum values at this time due most probably to the consumption of oxygen by the bacterial remineralization of OM.

In a review, [26] showed that this mechanism of seasonal decrease in oxygen concentration due to summer stratification, stagnation of water masses, and degradation of OM was present in similar environments, such as fjords and estuaries. Many studies point out that this natural mechanism can be amplified and reach critical levels for wildlife in response to human pressures and climate change, which enrich the marine environment with OM and increase the intensity or duration of stratification [3,4,27,28].

While the oxygen decreases observed in the deep layer in the Ushuaia Bay valley appear to be mainly the result of natural processes, it is feared that current salmon aquaculture projects and increased tourism activity will increase organic matter inputs at depth and increase the risk of hypoxia.

In the studied period, DO concentrations below 2 mg/L, which is usually considered as the threshold for hypoxia [4], were not observed. However, it has also been defined from a biological and ecological point as "DO [levels] that forces fish and aquatic invertebrates to either work harder at extracting oxygen from the water or reduce their rate of energy expenditure to match the availability of oxygen" [29]. For example, [5] define a threshold of 4.6 mg/L for which an impact on the physiology of crustaceans, up to a lethal effect, is observed. Our observations in the deep layer at the fixed station show that OD concentrations below this threshold of 4.6 mg/L were reached once, in June 2015. It is conceivable that such a reduction if repeated could affect marine wildlife in the Ushuaia Bay valley and also in the multiple small deep basins that lines the Beagle Channel.

The king crabs Lithodes santolla and Paralomis granulosa, represent a major touristic and economic resource for Argentina and Chile in the Beagle Channel [30]. Both species have benthic habitats as larvae and adults [30,31] and also show a strong sensibility to dissolved oxygen availability [6,32]. These species have been subjected to strong fishing pressures and despite the major efforts to restock them, the overall population of these crustaceans in the Beagle Channel is not showing positive trends [30]. The spatial and temporal patterns of dissolved oxygen distribution and potential depletion is the key to understanding the life traits and mobility of king crabs in the Beagle Channel and eventually to propose measures for repopulation and sustainable exploitation. Interdisciplinary research is needed to advance in that direction.

5. Conclusions

This is the first high spatial and seasonal resolution study of the physical and biogeochemical characteristics of Ushuaia Bay, with the objectives of understanding seasonal oxygen depletion and providing baseline data for future studies.

The major outcomes and conclusions of this study are:

- The seasonal stratification, observed during summer and autumn (December 2017–March2018), is induced mainly by freshwater inputs at the surface during snowmelt and is concomitance with planktonic production in the surface layer.
- Despite the inputs of organic matter of natural and urban origin by runoff, outside the most coastal part, the rest of Ushuaia Bay does not seem to be affected by these inputs because the rapid renewal of the bay's waters maintains a high level of oxygenation.
- The decrease in oxygen in the deep layer in the proximal part of the valley during summer and autumn is likely due to the settling and degradation of planktonic organic matter produced in the surface layer, that is found in the form of aggregates in the deep layer and low water turnover.
- It is likely that a seasonal decrease in dissolved oxygen also occurs in the multiple deep sub-basins that are present along the Beagle Channel, due to deep layer stagnation and surface organic production in stratified periods.

- The DO depletion might extend in time and space in line with global warming, glacier retreat and the subsequent increase of vertical stratification, and thus yield to significant alterations of this sub-Antarctic ecosystem.

Author Contributions: Conceptualization, methodology, and writing, X.F.M., J.M., X.D.d.M., F.B.; analysis, L.K., C.M., C.B.C., X.F.M., X.D.d.M., F.B., J.M.; funding acquisition, X.D.d.M., J.M. All authors have read and agreed to the published version of the manuscript.

Funding: This research was funded by the ECOS-SUD program in collaboration with SeCyT (Secretaría de Ciencia y Tecnología) for the project HYDRO-USHUAIA. This study was also supported by the Agencia Nacional de Promoción Científica y Tecnológica (PICT 2014/3106), Consejo Nacional de Investigaciones Científicas y Técnicas (P-UE 2016: 22920160100077CO CADIC, and the UPVD's BQR program.

Acknowledgments: We acknowledge the everlasting support and hard work at sea of CADIC's Nautical Service. Andrea Malits and Gustavo Lovrich are acknowledged for advice and support.

Conflicts of Interest: The authors declare no conflict of interest.

References

1. Wakeham, S.G.; Lee, C. Organic geochemistry of particulate matter in the ocean: The role of particles in oceanic sedimentary cycles. *Org. Geochem.* **1989**, *14*, 83–96, doi:10.1016/0146-638090022-3.
2. Syvitski, J.P.M.; Burrell, D.C.; Skei, J.M. *Fjords: Processes and Products*; Springer Science & Business Media: New York, NY, USA,1987; p. 379, doi:10.1002/jqs.3390040311.
3. Zhang, J.; Gilbert, D.; Gooday, A.J.; Levin, L.; Naqvi, S.W.A.; Middelburg, J.J.; Van Der Plas, A.K. Natural and human-induced hypoxia and consequences for coastal areas: Synthesis and future development. *Biogeosciences* **2010**, *7*, 1443–1467, doi:10.5194/bg-7-1443-2010.
4. Diaz, R.J.; Rosenberg, R. Marine benthic hypoxia: A review of its ecological effects and the behavioural responses of benthic macrofauna. *Oceanogr. Mar. Biol. Annu. Rev.* **1995**, *33*, 245–303.
5. Vaquer-Sunyer, R.; Duarte, C.M. Thresholds of hypoxia for marine biodiversity. *Proc. Natl. Acad. Sci. USA* **2008**, *105*, 15452–15457, doi:10.1073/pnas.0803833105.
6. Paschke, K.; Cumillaf, J.P.; Loyola, S.; Gebauer, P.; Urbina, M.; Chimal, M.E.; Rosas, C. Effect of dissolved oxygen level on respiratory metabolism, nutritional physiology, and immune condition of southern king crab *Lithodes santolla* (Molina, 1782) (Decapoda, Lithodidae). *Mar. Biol.* **2010**, *157*, 7–18, doi:10.1007/s00227-009-1291-1.
7. Freeland, H.J.; Farmer, D.M.; Levings, C.D. Fjord Oceanography. In Proceedings of the NATO Conference on Fjord Oceanography, Victoria, BC, Canada, 4–8 June 1979; Plenum Press: New York, NY, USA; London, UK, 1980; p. 715.
8. Isla, F.; Bujalesky, G.; Coronato, A. Procesos estuarinos en el canal Beagle, Tierra del Fuego Estuarine. *Rev. Asoc. Geol. Argent.* **1999**, *54*, 307–318.
9. Bujalesky, G.; Aliotta, S.; Isla, F. Facies del subfondo del canal Beagle, Tierra del Fuego. *Rev. Asoc. Geológica Argent.* **2004**, *59*, 29–37.
10. Iturraspe, R.J.; Sottini, R.; Schroeder, C.; Escobar, J. Hidrología y variables climáticas del Territorio de Tierra del Fuego. Información básica. *Contrib. Científica CADIC* **1989**, *7*, 196.
11. Balestrini, C.; Manzella, G.; Lovrich, G.A. Simulación de corrientes en el Canal Beagle y Bahía Ushuaia, mediante un modelo bidimensional. *Serv. Hidrogr. Nav.* **1998**, *98*, 1–58.
12. Bujalesky, G.G. The flood of the Beagle Valley (11,000 YR B.P.), Tierra del Fuego. *An. Inst. Patagon.* **2011**, *39*, 5–21, doi:10.4067/s0718-686X2011000100001.
13. Amin, O.; Comoglio, L.; Spetter, C.; Duarte, C.; Asteasuain, R.; Freije, R.H.; Marcovecchio, J. Assessment of land influence on a high-latitude marine coastal system: Tierra del Fuego, southernmost Argentina. *Environ. Monit. Assess.* **2011**, *175*, 63–73, doi:10.1007/s10661-010-1493-5.
14. Torres, A.I.; Gil, M.N.; Amín, O.A.; Esteves, J.L. Environmental characterization of a eutrophicated semi-enclosed system: Nutrient budget (Encerrada Bay, Tierra del Fuego Island, Patagonia, Argentina). *Water Air Soil Pollut.* **2009**, *204*, 259–270, doi:10.1007/s11270-009-0042-8.
15. Martín, J.; Colloca, C.; Diodato, S.; Malits, A. Variabilidad espacio-temporal de las concentraciones de oxígeno disuelto en Bahía Ushuaia y Canal Beagle (Tierra del Fuego). *Nat. Patagónica* **2016**, *8*, 193.

16. Schlitzer, R. Ocean Data View. 2019. Available online: https://odv.awi.de (accessed on 28 October 2019).
17. Agrawal, Y.C.; Pottsmith, H.C. Instruments for particle size and settling velocity ob-servations in sediment transport. *Mar. Geol.* **2000**, *168*, 89–114, doi:10. 1016/S0025-322700044-X.
18. Agrawal, Y.C.; Whitmire, A.; Mikkelsen, O.A.; Pottsmith, H.C. Light scattering by random shaped particles and consequences on measuring suspended sediments by laser diffraction. *J. Geophys. Res.* **2008**, *113*, doi:10.1029/2007JC004403.
19. Traykovski, P.; Latter, R.J.; Irish, J.D. A laboratory evaluation of the laser in situ scat-tering and transmissometery instrument using natural sediments. *Mar. Geol.* **1999**, *159*, 355–367, doi:10.1016/S0025-322700196-0.
20. Mikkelsen, O.A.; Hill, P.S.; Milligan, T.G.; Chant, R.J. In situ particle size distributions and volume concentrations from a LISST-100 laser particle sizer and a digital floc camera. *Cont. Shelf Res.* **2005**, *25*, 1959–1978, doi:10.1016/j.csr.2005. 07.001.
21. Graham, G.W.; Smith, W.A.M. The application of holography to the analysis of size and settling velocity of suspended cohesive sediments. *Limnol. Oceanogr. Methods* **2010**, *8*, 1–15, doi:10.4319/lom.2010.8.1.
22. Aminot, A.; Kérouel, R. *Hydrologie des Écosystèmes Marins: Paramètres et Analyses*; Editions Quae; INRA: Versailles, France, 2004; p. 336.
23. Balestrini, C.F.; Vinuesa, J.; Speroni, J.; Lovrich, G.; Mattenet, C.; Cantu, C.; Medina, P. Estudio de las Corrientes Marinas en los alrededores de la Península Ushuaia. *Comun. Científica CADIC* **1990**, 10, pp. 1–33.
24. Schneider, W.; Pérez-Santos, I.; Ross, L.; Bravo, L.; Seguel, R.; Hernández, F. On the hydrography of Puyuhuapi Channel, Chilean Patagonia. *Prog. Oceanogr.* **2014**, *129*, 8–18, doi:10.1016/j.pocean.2014.03.007.
25. Gil, M.N.; Torres, A.I.; Amin, O.; Esteves, J.L. Assessment of recent sediment influence in an urban polluted subantarctic coastal ecosystem. Beagle Channel (Southern Argentina). *Mar. Pollut. Bull.* **2011**, *62*, 201–207, doi:10.1016/j.marpolbul.2010.10.004.
26. Björk, G.; Nordberg, K.; Arneborg, L.; Bornmalm, L.; Harland, R.; Robijn, A.; Ödalen, M. Seasonal oxygen depletion in a shallow sill fjord on the Swedish west coast. *J. Mar. Syst.* **2017**, *175*, 1–14, doi:10.1016/j.jmarsys.2017.06.004.
27. Caballero-Alfonso, A.M.; Carstensen, J.; Conley, D.J. Biogeochemical and environmental drivers of coastal hypoxia. *J. Mar. Syst.* **2015**, *141*, 190–199, doi:10.1016/j.jmarsys.2014.04.008.
28. Breitburg, D.; Levin, L.A.; Oschlies, A.; Grégoire, M.; Chavez, F.P.; Conley, D.J.; Zhang, J. Declining oxygen in the global ocean and coastal waters. *Science* **2018**, *359*, doi:10.1126/science.aam7240.
29. Thomas, Y.; Flye-Sainte-Marie, J.; Chabot, D.; Aguirre-Velarde, A.; Marques, G.M.; Pecquerie, L. Effects of hypoxia on metabolic functions in marine organisms: Observed patterns and modeling assumptions within the context of Dynamic Energy Budget (DEB) theory. *J. Sea Res.* **2019**, *143*, 231–242, doi:10.1016/j.seares.2018.05.001.
30. Lovrich, G.A.; Tapella, F.; Di Salvatore, P.; Gowland-Sainz, M.F.; Diez, M.J.; Fernández, A.L.; Sotelano, M.P.; Romero, M.C.; Negri, M.F.; Chiesa, I.; et al. Estado poblacional de la centolla *Lithodes santolla* en el Canal Beagle—2016—Cluster de Pesca Artesanal de Tierra del Fuego. In *Cluster de Pesca Artesanal de Tierra del Fuego Convenio Específico de Asistencia Técnica CONICET-UNTDF (Res 361/15)*; Researchgate: Ushuaia, Argentina, 2017; p. 85, doi:10.13140/RG.2.2.25514.52165/1.
31. Tapella, F.; Lovrich, G.A. Asentamiento de estadios tempranos de las centollas *Lithodes santolla* y *Paralomis granulosa* (Decapoda: Lithodidae) en colectores artificiales pasivos en el Canal Beagle, Argentina. *Investig. Mar.* **2006**, *34*, 47–55, doi:10.4067/S0717-71782006000200005.
32. Urbina, M.A.; Paschke, K.; Gebauer, P.; Cumillaf, J.P.; Rosas, C. Physiological responses of the southern king crab, *Lithodes santolla* (Decapoda: Lithodidae), to aerial exposure. *Comp. Biochem. Physiol. Part A Mol. Integr. Physiol.* **2013**, *166*, 538–545, doi:10.1016/j.cbpa.2013.08.006.